J Mater Sci: Mater Med (2010) 21:3119–3127
DOI 10.1007/s10856-010-4166-6

Indirect rapid prototyping of biphasic calcium phosphate scaffolds as bone substitutes: influence of phase composition, macroporosity and pore geometry on mechanical properties

M. Schumacher · U. Deisinger · R. Detsch · G. Ziegler

Received: 14 June 2010 / Accepted: 21 September 2010 / Published online: 15 October 2010

Abstract While various materials have been developed for bone substitute and bone tissue engineering applications over the last decades, processing techniques meeting the high demands of scaffold shaping are still under development. Individually adapted and mechanically optimised scaffolds can be derived from calcium phosphate (CaP-) ceramics via rapid prototyping (RP). In this study, porous ceramic scaffolds with a periodic pattern of interconnecting pores were prepared from hydroxyapatite, β-tricalcium phosphate and biphasic calcium phosphates using a negative-mould RP technique. Moulds predetermining various pore patterns (round and square cross section, perpendicular and 60° inclined orientation) were manufactured via a wax printer and subsequently impregnated with CaP-ceramic slurries. Different pore patterns resulted in macroporosity values ranging from about 26.0–71.9 vol% with pore diameters of approximately 340 µm. Compressive strength of the specimens (1.3–27.6 MPa) was found to be mainly influenced by the phase composition as well as the macroporosity, both exceeding the influence of the pore geometry. A maximum was found for scaffolds with 60 wt% hydroxyapatite and 26.0 vol% open porosity. It has been shown that wax ink-jet printing allows to process CaP-ceramic into scaffolds with highly defined geometry, exhibiting strength values that can be adjusted by phase composition and pore geometry. This strength level is within and above the range of human cancellous bone. Therefore, this technique is well suited to manufacture scaffolds for bone tissue engineering.

M. Schumacher (✉) · U. Deisinger · G. Ziegler
Friedrich-Baur-Research Institute for Biomaterials, University of Bayreuth, 95440 Bayreuth, Germany
e-mail: matthias.schumacher@fbi-biomaterialien.de

U. Deisinger
e-mail: ulrike.deisinger@fbi-biomaterialien.de

G. Ziegler
e-mail: guenter.ziegler@biocer-gmbh.de

R. Detsch · G. Ziegler
BioCer Entwicklungs-GmbH, 95447 Bayreuth, Germany
e-mail: rainer.detsch@biocer-gmbh.de

1 Introduction

Bone grafting is an important issue in regenerative medicine today, but still the majority of bone grafting procedures use natural bone material from auto- or allografts as bone substitute material. The major drawbacks of these materials are their limited availability, donor site morbidity and the risk of infection or transfer of diseases. Hence, the demand for synthetic bone graft materials increases [1, 2].

Calcium phosphate ceramics have been established as synthetic bone substitute materials over the last decades [3, 4]. Since the chemical composition of hydroxyapatite, as a typical calcium phosphate ceramic, is quite similar to the inorganic part of natural bone, these materials offer excellent biocompatibility and cause no inflammatory response. Hydroxyapatite $Ca_5(PO_4)_3OH$ (HA) and β-tricalcium phosphate $Ca_3(PO_4)_2$ (β-TCP), differing in their Ca/P ratio, are the most important calcium phosphate ceramics in medical applications, being both biocompatible and osteoconductive. Compressive strength values for dense HA and β-TCP ceramics derived from the literature vary from 138 to 900 and 315 to 750 MPa, respectively [5–11]. The wide range of strength values results from different raw materials, sample preparation techniques, sintering conditions and analysis setups [12]. Biphasic calcium phosphate ceramics (BCP) offer the possibility to vary this ratio on average and, therefore, tailor the

characteristics of the biomaterial [9, 13, 14]. Several studies have shown that the Ca/P ratio has a strong impact on the potential of the materials in vitro and in vivo, e.g. the solubility of β-TCP in physiologic environment in contrast to the almost non-soluble HA [15, 16].

Nowadays, calcium phosphate ceramics of varying phase composition are applied in the form of bone cements, granulates or blocks of different sizes and shapes [12, 16]. Furthermore, special focus has been given to macroporous ceramics, since it is general consensus that open porosity is crucial for the incorporation of a bone substitute into the living bone tissue [17]. Various studies on in vitro and in vivo cell ingrowth, nutrient supply via diffusion and vascularisation of porous implants revealed a pore size in the range of 100–800 μm and an open porosity above 50 vol% as ideal for bone ingrowth [18, 19]. Such macroporosity has, besides the phase composition and pore characteristics like diameter, distribution, interconnectivity and morphology, a strong impact on the strength of the bone substitute, since it disrupts the mechanical integrity of the material [18]. Numerous studies suggest an exponential decrease of compressive strength with increasing porosity [9, 18, 20–22].

Zyman et al. [23] measured the compressive strength of micro-porous (3–6 vol%) BCP ceramics of varying phase ratio as 420–591 MPa, increasing with the TCP content. At higher porosities, controversial results have been published. While Kwon et al. found lower compressive strength values for TCP and BCP ceramic samples of 65–90 vol% porosity compared to HA [24], a strength maximum of 3.3–5.8 MPa has been found for 60–70 vol% porous BCP ceramics with approx. 60 wt% HA by Guo et al. [25]. A strengthening effect of small quantities of TCP in BCP ceramics under bending load has also been described by Raynaud et al. for BCP ceramics with a molar HA/TCP ratio of 90/10 (3-point bending strength) [26] and by Royer et al. using biaxial flexure testing [27]. Other groups reported the compressive strength of porous BCP ceramics as 13.9–16.2 MPa (50 vol% porosity, 60/40 HA/TCP) [28] or 6.4 MPa for 65 vol% porous, microwave-sintered BCP ceramics [29]. Puértolas et al. recently measured the compressive strength of porous BCP ceramics as 3–4 and 9-12 MPa for BCP ceramic samples (27 wt% HA and 73 wt% β-TCP) with 31 vol% micro- and 34 vol% micro- and macro-porosity, respectively [30].

In most cases porosity is induced into synthetic biomaterials by techniques resulting in a statistic pore size and pore pattern distribution, like gas foaming [31], particulate leaching [20] and foam replica technique [24, 32]. While with these techniques porous architectures of only limited variability can be realised, rapid prototyping (RP) techniques are being adapted for the production of porous ceramics with well-defined architecture. Various direct RP methods, like ink-jet and three-dimensional printing [33–35] or dispense-plotting [36, 37] are used to manufacture complex shaped scaffolds from biocompatible materials like calcium phosphate ceramics or degradable polymers. Indirect RP or "lost mould techniques", on the other hand, use RP techniques to obtain a negative mould, which is subsequently filled with castables (e.g. ceramic slurry) and then removed from the dried body. Since the mould preparation is independent from the casting process and material, indirect RP can be adapted to a broad variety of scaffold materials. Moulds made by stereolithography have been employed to manufacture HA scaffolds via slurry casting with pores of square cross section and a size between 334 and 500 μm [38, 39]. Samples from TCP, HA and ceramic/polymer composites (e.g. TCP/polyethylene glycol) have been successfully manufactured by impregnation of RP derived wax moulds with linear pore channels of varying cross section and diameters between 150 and 2,000 μm [40–44]. Consequently, if an appropriate slurry system exists, the high resolution and accuracy of this RP technique could possibly be transferred to the scaffold.

In this work, wax ink-jet printing was used to manufacture negative moulds in order to obtain porous scaffolds from HA, β-TCP and biphasic ceramics with HA/TCP weight ratios of 80/20, 60/40, 40/60 and 20/80. Negative moulds were designed with a periodic pattern of intersecting, round- or square-shaped struts, predetermining an open macroporosity of 26.0–71.9 vol% in the final ceramic. Scaffolds were manufactured by impregnating the wax moulds with low viscosity ceramic slurry. After sintering at 1,300°C, phase analysis by RAMAN spectroscopy and X-ray diffraction as well as uniaxial compression testing were performed to evaluate (A) the dependency of phase composition and compressive strength, (B) the influence of pore shape, and (C) macroporosity on compressive strength.

2 Materials and methods

2.1 Preparation of specimens

CaP-specimens were manufactured using a negative mould technique involving wax ink-jet printing. This indirect rapid prototyping technique is a two-step process: first, an inverted model of the desired structure is designed using a 3D CAD system and produced from polymer wax using a wax printer. Molten wax is printed drop-wise layer by layer on a building platform by a moving print head, using build wax for the mould itself and support wax to fill voids. After one layer is completed, the wax is milled to a predefined slice thickness, the building platform is lowered and the next layer is printed. Once the printing process is finished,

the support wax is removed by a solvent. In a second step, the negative model is used as mould for casting of a low viscosity ceramic slurry, impregnating the negative mould. The wax is removed by pyrolysis during thermal treatment and the ceramic is sintered. The process steps are shown in the flowchart in fig. 1.

Three test series were designed to investigate (A) the compressive strength depending on the phase composition, (B) the influence of macroporosity, and (C) pore geometry on the strength of samples.

2.2 Mould design and preparation

Specimens were designed as cuboids with a three-dimensional periodic structure of pores using commercially available CAD software (Solid Works 2007). Samples with perpendicularly arranged pores with round-shaped cross section (R90) and varying strut diameters were designed with an open macroporosity value of 26.0, 32.3 and 71.9 vol%. Furthermore, perpendicular and 60° altering patterns of pores with square cross section (S90 and S60) were designed (Fig. 2), resembling scaffolds manufactured by another RP technique (dispense-plotting) described elsewhere [38]. Such pore configurations resulted in a macroporosity of 29.6 and 48.7 vol%, respectively. Pore diameter was kept constant at 340 µm consistently for all sample configurations.

The CAD models were inverted to generate a negative mould for the subsequent casting process. The models were sliced in layers of 13 µm thickness and the pattern of build and support wax was calculated for each layer. Wax moulds were produced using a wax ink-jet printing machine (BT66, Solidscape Inc.). After the printing process was completed, the support wax was removed using a specific solvent (Solidscape Inc.).

2.3 Casting and sintering

Raw powders of hydroxyapatite and tricalcium phosphate were derived from Merck, Germany, and calcined for 1 h at 900°C to reduce the specific surface area [45], thus decreasing the viscosity of the slurry and permitting a higher solids loading of the slurry. Biphasic mixtures with HA/TCP weight ratios of 80/20, 60/40, 40/60 and 20/80 were prepared of untreated powders before calcination. Biphasic CaP samples are referred to as HA80, HA60, HA40 and HA20, respectively.

A slurry with 60 wt% solids loading was prepared by dispersing calcined powder in distilled water, adding a total of 5.5 wt% of organic additives to improve flowability of the slurry and green part strength. The slurry was ball-milled to break agglomerates and stirred overnight prior to casting. Wax moulds were completely filled with ceramic slurry and entrapped air was removed by applying vacuum. Specimens were dried at room temperature and, subsequently, sintered at 1,300°C for 2 h. During heating, a dwell time was set at 500°C to account for pyrolysis of wax and organic additives.

Samples with R90 geometry (26.0 vol% open porosity) were produced from all ceramic materials to investigate the influence of phase composition on compressive strength (test series A), whereas other pore configurations were only produced from HA60 to evaluate the influence of macroporosity (R90, test series B) and different pore structure modifications on mechanical characteristics (S90 and S60, test series C).

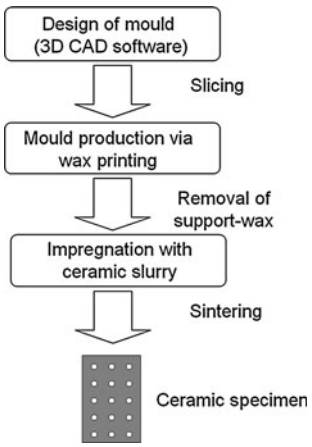

Fig. 1 Processing steps of the indirect RP technique involving wax ink-jet printing

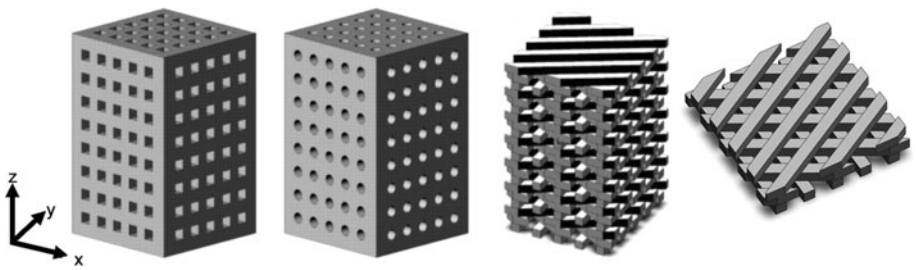

Fig. 2 Design of the specimens: cubic with perpendicularly arranged round- (R90, *left*) and square-(S90, *middle*) shaped pores and with square shaped pores in 60° altering layers (including detailed view, S60, *right*)

2.4 Characterisation

Phase composition of sintered bodies was determined by RAMAN spectroscopy (LABRAM, Jobin–Yvon Horiba) and X-ray diffraction (XRD). Therefore, samples were powdered using an agate mortar and pestle. Data collection was performed in the range of $2\theta = 25$–$41°$ in increments of 0.02° using a Seifert 3000P diffractometer using Cu-Kα radiation ($\lambda = 1.5418$ Å). Scanning electron microscopy (SEM, Quanta 200, FEI) was used to observe surface characteristics of wax moulds and ceramic samples. Dimensions of all samples were measured using a stereo microscope (MZM1, Askania, Mikroskop Technik Rathenow) and graphical analysing software (analySIS, Soft Imaging Systems Corp.) before and after sintering to determine the shrinkage. Density of all specimens was measured using a helium-pycnometer (AccuPyc 1330, Micromeritics).

Compressive strength of all samples was determined using an Instron testing machine (Instron 1362) fitted with a 5 kN load cell. The load rate was set to 1 mm/min. A total of 5 samples of each geometry and material were tested.

2.5 Statistical evaluation

Data analysis was performed using standard linear regression algorithms (Origin 6.1G, Origin Lab. Corp.).

3 Results and discussion

3.1 Phase composition

RAMAN spectra of mono- and biphasic calcium phosphate ceramics sintered at 1300°C for 2 h are shown in Fig. 3. The peak pattern of HA and TCP confirm the phase-purity of both materials. The biphasic nature of the other samples can be seen from their peak pattern, resulting from a superposition of pure HA and β-TCP peaks and indicating the gradual change in phase composition.

Results of XRD analysis are shown in Fig. 4. Phase-pure HA (XRD JCPDS file No. 09-0432) and β-TCP (No. 09-0169) were found for HA and TCP samples, respectively. A gradual change in phase composition was found in case of the biphasic ceramic samples, exhibiting the characteristic peaks of HA and TCP in varying intensities.

3.2 Geometrical analysis

SEM micrographs of wax moulds after removal of the support wax reveal an anisotropic surface structure. As a result of the layer-by-layer process of wax printing and milling of each wax layer, surfaces perpendicular to the building platform are highly textured (Fig. 5a), whereas surfaces parallel to the building platform have no significant roughness (Fig. 5c). Micrographs of sintered ceramic bodies (Fig. 5b, d) reveal a surface texture similar to the negative mould, indicating the high accuracy of the casting process.

A photograph of R90 samples with different HA/TCP ratios is shown in Fig. 6. All samples had an interconnecting, open pore network.

High dimensional accuracy was found for all samples. Only R90 samples produced from HA40 and HA20

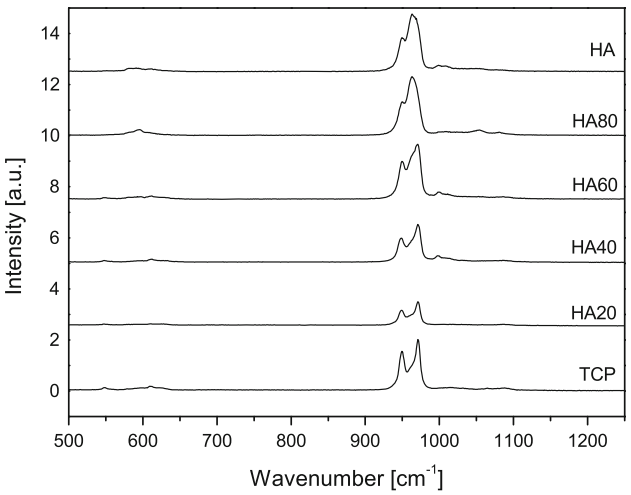

Fig. 3 RAMAN spectra of sintered mono- and biphasic calcium phosphate ceramics, showing the gradual change in phase composition from pure HA (*top*) to TCP (*bottom*)

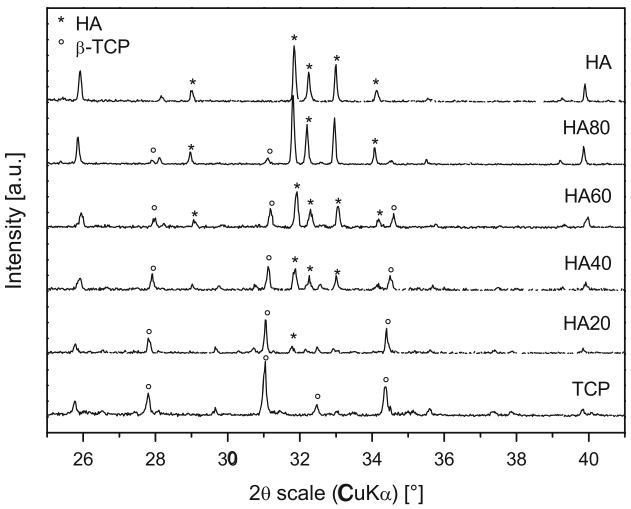

Fig. 4 X-ray diffraction data of powdered mono- and biphasic calcium phosphate ceramics, showing the gradual change in phase composition from pure HA (*top*) to pure β-TCP (*bottom*)

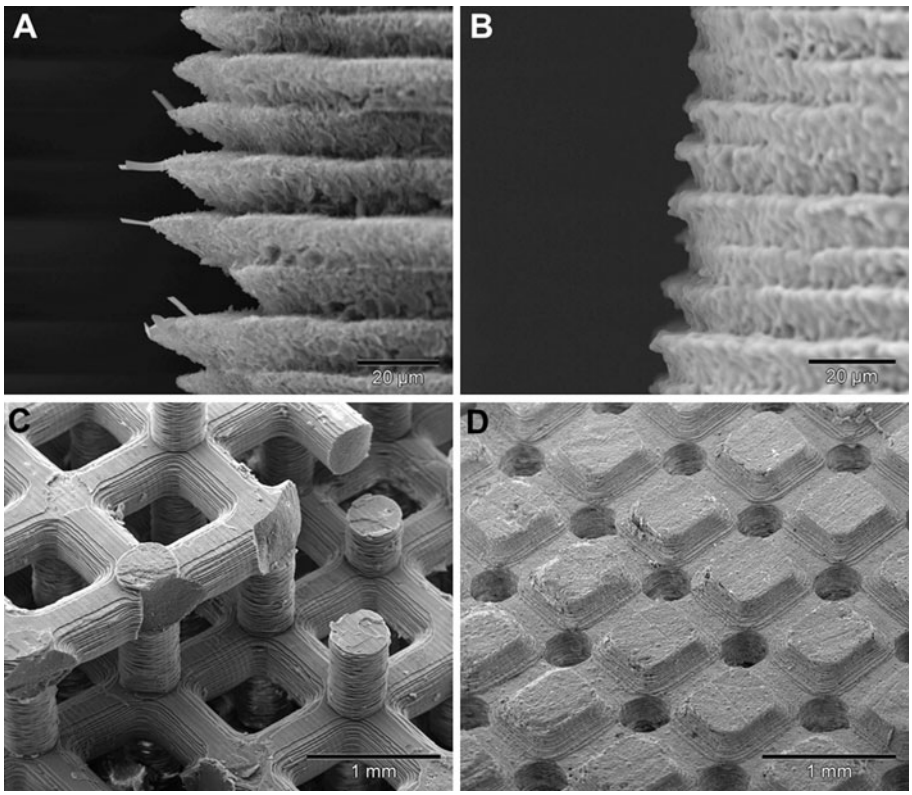

Fig. 5 SEM micrographs of R90 wax moulds, representing a highly textured surface perpendicular to the building platform (**a**, **c**). Sintered ceramic specimens (**b**, **d**) show the same surface texture, indicating the accuracy of the casting process

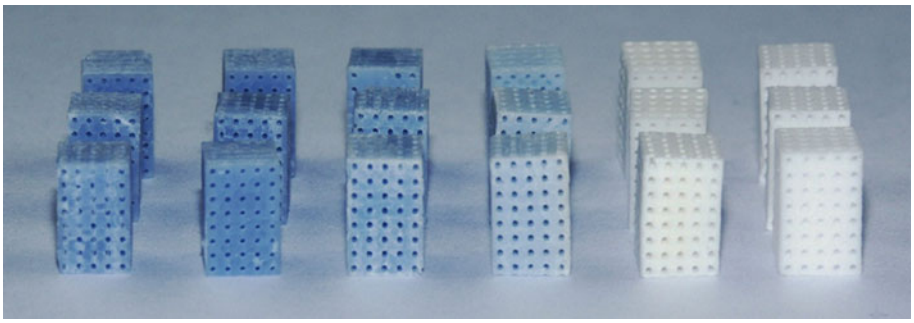

Fig. 6 Photograph of R90 samples manufactured from HA, HA80, HA60, HA40, HA20 and TCP (*left to right*)

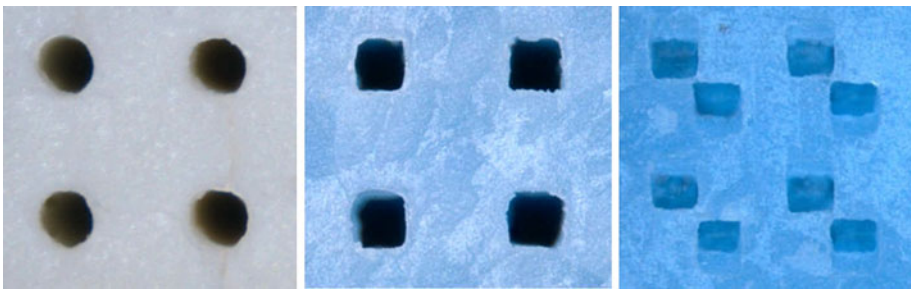

Fig. 7 Micrographs of sintered specimens show the round and square pore geometry of R90 (*left*), S90 (*middle*) and S60 (*right*, lateral view) samples

revealed a slight distortion after sintering resulting in non-parallel surfaces in the x/y-plane (Fig. 6, 2nd and 3rd sample from right). This may be a result of a density gradient established during casting or a temperature gradient that occurred during sintering. However, such distortion could have strong influence on the results of the subsequent compression testing.

All pores had the predetermined shape (Fig. 7). Pore diameters (Table 1) as well as absolute dimensions of the sintered specimens differed between the different

Table 1 Bulk density and pore diameters (round cross section) of sintered ceramic samples (R90)

Sample	HA	HA80	HA60	HA40	HA20	TCP
HA/TCP weight ratio	100/0	80/20	60/40	40/60	20/80	0/100
Pore diameter (μm)	335.3 ± 15.7	316.1 ± 14.3	363.3 ± 15.3	342.0 ± 19.1	333.1 ± 12.3	320.2 ± 20.3
Bulk density (% th. d.)	95.6 ± 0.7	93.8 ± 1.0	94.9 ± 2.2	93.9 ± 0.5	95.6 ± 0.2	97.9 ± 0.6

materials, since no individually adapted wax moulds were used for each material.

However, variance within each material was very low (below 6.3% in pore diameter), confirming the high accuracy and reproducibility of the moulding technique.

Shrinkage was calculated as 26.3% for HA and 15.1% for β-TCP samples during sintering for 2 h at 1,300°C. For biphasic mixtures, shrinkage decreased with decreasing HA/TCP ratio in an almost linear manner (Fig. 8).

Bulk density of R90 samples was determined to values between 94 and 98% th.d. by pycnometry (Table 1). This variance can be accounted to closed micro pores within the specimens.

3.3 Compressive strength

The influence of phase composition on compressive strength was investigated using R90 specimens of varying phase composition (test series A). Additionally, R90 samples with varying macroporosity manufactured from HA60 ceramic were used to correlate macroporosity to compressive strength (test series B). Finally, the effect of different pore geometries was analysed using R90, S90 and S60 biphasic (HA60) samples (test series C).

In test series A, a significantly higher strength compared to single phase samples was found for the HA-rich BCP ceramics HA80 (18.4 ± 3.8 MPa) and HA60 (27.6 ± 4.5 MPa), which exhibited the highest strength value (Fig. 9). These results correlate to the findings of Guo et al., who found a similar maximum for porous HA/TCP 60/40 ceramics [25]. Contrary to the strength values of CaP ceramics found in literature, the strength of pure HA samples (8.5 ± 3.1 MPa) was less than that of pure TCP samples (9.6 ± 1.5 MPa), although the results were not significantly different. This may be due to cracks, which were found to be more distinct in HA specimens than in BCP and were not observed in TCP samples at all. HA40 and HA20 specimens revealed low strength, 8.5 ± 1.8 and 5.6 ± 1.6 MPa, respectively. Besides from the generally lower strength of TCP, this may result from the distortion of these samples described above. Due to the non-parallel surfaces no homogeneous load level could develop within the ceramic. This is stressed by observations during the compression test, showing that collapse of these samples started at their bent surface. In case of non-deformed samples, failure planes developed parallel to the load direction and brittle crushing occurred from pore layer to pore layer on random faces of the sample. This

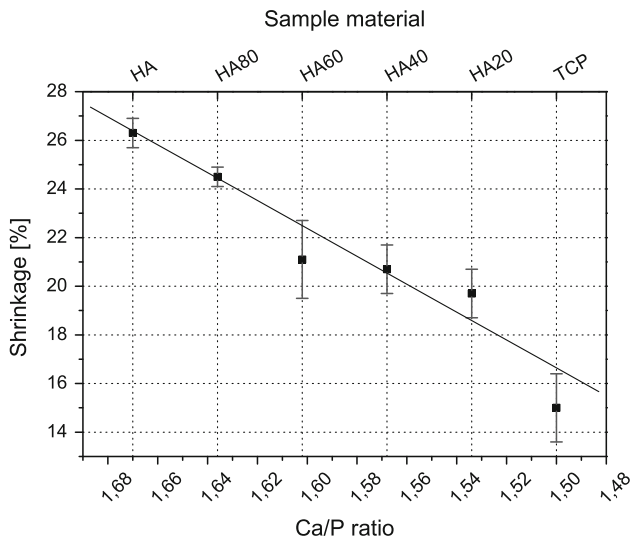

Fig. 8 Influence of phase composition on the shrinkage (z-axis) after sintering at 1,300°C for 2 h

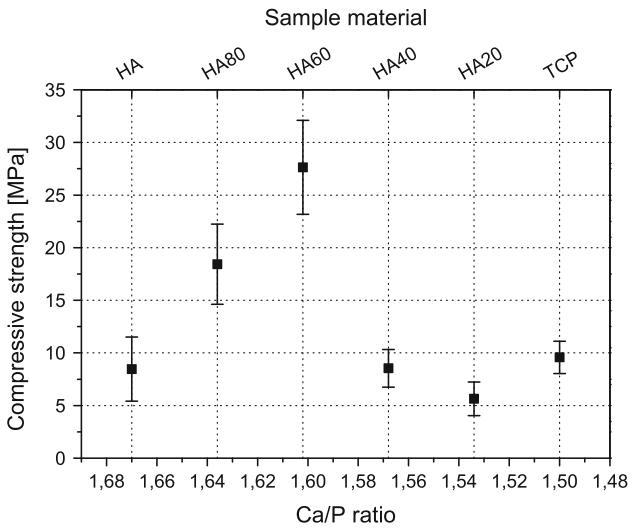

Fig. 9 Influence of phase composition on the compressive strength of biphasic calcium phosphate ceramic specimens with interconnecting, round-shaped pores (R90, pore diameter approx. 340 μm, 26 vol% open porosity)

corresponds to failure mechanisms described in literature, assuming that failure of porous brittle materials occurs due to stress superposition between repetitively arranged pores [46, 47].

During testing of R90 samples with varying macroporosity (test series B), strength was found to decrease with increasing porosity of the samples. Compressive strength values of 27.6, 19.7 and 1.6 MPa were measured for samples with 26.0, 32.3 and 71.9 vol% open porosity, respectively (Fig. 10).

Linear regression revealed the following exponential relation (Eq.1) between porosity and compressive strength (σ_c compressive strength, ε_{open} open porosity).

$$ln\sigma_c = -A.\varepsilon_{open} + B \quad \text{(Eq.1)}$$

The regression coefficients A and B in this study were calculated to $A = 0.067$ and $B = 5.053$, which corresponds well to data published by Metsger et al. [9].

Compressive testing of biphasic calcium phosphate ceramic (HA60) specimens with differently shaped and oriented pores (test series C) revealed a lower strength of S90 compared to R90 samples (Table 2).

This could be related to the pore geometry, either to stress concentrations in salient angles of samples with square pore cross section or the generally higher open porosity of samples with square-shaped pore cross sections but otherwise identical pore and strut dimensions. A further decrease in compressive strength was found for S60 samples (9.9 ± 2.9 MPa), which may also be due to the complex pore network in S60 samples with more salient angles but also to the higher porosity of these samples (48.7 vol%) compared to S90 samples (29.6 vol%).

As shown in Fig. 10, strength values found in test series C show only little deviation from the regression line described by Eq.1. This suggests a major effect of porosity and only secondary influence of pore geometry on the compressive strength.

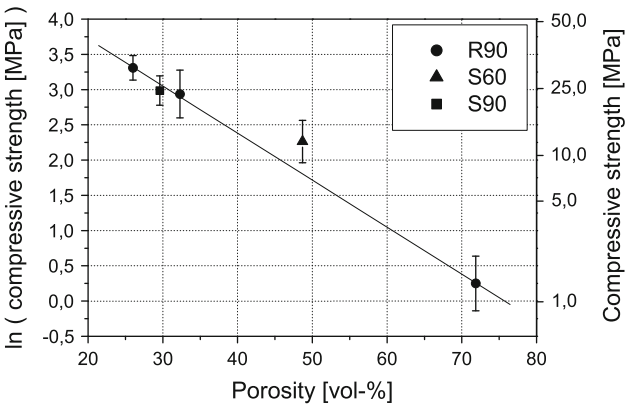

Fig. 10 Influence of open porosity and pore geometry on the compressive strength of BCP scaffolds (HA/TCP ratio 60/40). Pore diameter was approx. 340 μm for all pore configurations

Table 2 Compressive strength and open porosity of sintered HA60 scaffolds with different pore configurations: round-(R90) or square-(S90, S60) shaped pore cross sections with either orthogonal (R90, S90) pore orientation or pores arranged in 60° altering layers (S60)

Sample geometry	R90	S90	S60
Compressive strength (MPa)	27.6 ± 4.5	20.2 ± 4.3	9.9 ± 2.9
Open porosity (vol%)	26.0	29.6	48.7

Specimens in all test series attained a compressive strength within and above the range of human cancellous bone (0.6–15 MPa [4, 48]). The indirect rapid prototyping technique described in this study is therefore well suited for the production of calcium phosphate scaffolds for bone repair. The application of scaffolds manufactured in that way for bone tissue engineering has already been shown [49].

4 Summary and conclusion

In this study it was shown that macroporous mono- and biphasic calcium phosphate ceramic scaffolds for bone replacement and bone tissue engineering can be manufactured with variable pore design in high accuracy by a negative mould technique involving wax ink-jet printing. The phase composition of the ceramic can be varied between pure HA and β-TCP without changing the process parameters, making it possible to improve the mechanical and bioactive properties of the implant. In this study, a maximum strength of 27.6 MPa was found for samples with round-shaped pores and a porosity of 26.0 vol%, produced from a biphasic calcium phosphate ceramic with 60 wt% hydroxyapatite and 40 wt% β-tricalcium phosphate (HA60). Less strength was measured for other biphasic mixtures and single phase calcium phosphate ceramics. Compression testing of samples with similar pore configuration but higher porosity values revealed an exponential dependency between macroporosity and strength, indicating the possibility to pre-estimate the strength of a porous implant. Variations of pore cross section and orientation, comprising an increase in open porosity, resulted in a further decrease of the samples compressive strength. However, the dependency between macroporosity and compressive strength apparently exceeded the effect of pore geometry. Nevertheless, all samples had a strength within and above the range frequently given for human cancellous bone (0.6–15 MPa).

Since the RP technique described in this paper is based on CAD data, medical imaging techniques like computed tomography (CT) could be used as data source, establishing

the possibility to manufacture patient-specific bone grafts or bone tissue engineering constructs. Thereby, the mechanical properties of the implant can be adapted by coordinated variation of phase composition and geometrical design to the individual requirements. Furthermore, the implant integration can be optimised by the same variations, since the phase composition influences the growth and differentiation of bone cells. The pore size is also well known to be crucial for tissue ingrowth and vascularisation. Recent studies have shown a distinct influence of the pore shape on cell growth behaviour in vitro [50]. This indicates, that the presented indirect rapid prototyping technique is well suited for the production of calcium phosphate bone graft substitutes and scaffolds for bone tissue engineering, as it allows control of porosity, pore design and external shape of an implant of any desired HA/TCP phase ratio.

References

1. Damien CJ, Parsons JR. Bone graft and bone graft substitutes: a review of current technology and applications. J Appl Biomater. 1991;2:187–208.
2. Habibovic P, de Groot K. Osteoinductive biomaterials—properties and relevance in bone repair. J Tissue Eng Regen Med. 2007;1:25–32.
3. Dorozhkin S, Epple M. Biological and medical significance of calcium phosphates. Angew Chem Int Ed Engl. 2002;41: 3130–46.
4. Hing KH. Bone repair in the twenty-first century: biology, chemistry or engineering? Philos Transact A Math Phys Eng Sci. 2004;326:2821–50.
5. Rao WR, Boehm RF. A study of sintered apatites. J Dent Res. 1974;53:1351–4.
6. De With G, Van Dijk HJA, Hattu N, Prijs K. Preparation, microstructure and mechanical properties of dense polycrystalline hydroxy apatite. J Mater Sci. 1981;16:1592–8.
7. Dorozhkin SV. Bioceramics of calcium orthophosphates. Biomaterials. 2009;31(7):1465–85.
8. Akao M, Aoki H, Kato K. Mechanical properties of sintered hydroxyapatite for prosthetic applications. J Mater Sci. 1981; 16:809–12.
9. Metsger DS, Rieger MR, Foreman DW. Mechanical properties of sintered hydroxyapatite and tricalcium phosphate ceramic. J Mater Sci Mater Med. 1999;10:9–17.
10. Driessen AA, Klein CP, de Groot K. Preparation and some properties of sintered beta-whitlockite. Biomaterials. 1982;3: 113–6.
11. Jarcho M, Bolen CH, Thomas MB, Bobick J, Kay JF, Doremus RH. Hydroxylapatite synthesis and characterization in dense polycrystalline form. Synthesis and fabrication of β-tricalcium phosphate (whitlockite) ceramics for potential prosthetic applications. J Mater Sci. 1979;14:142–50.
12. Daculsi G. Biphasic calcium phosphate concept applied to artificial bone, implant coating and injectable bone substitute. Biomaterials. 1998;19:1473–8.
13. Alam MI, Asahina I, Ohmamiuda K, Takahashi K, Yokota S, Enomoto S. Evaluation of ceramics composed of different hydroxyapatite to tricalcium phosphate ratios as carriers for rhBMP-2. Biomaterials. 2001;22:1643–51.
14. Rice JM, Hunt JA, Gallagher JA. Quantitative evaluation of the biocompatible and osteogenic properties of a range of biphasic calcium phosphate (BCP) granules using primary cultures of human osteoblasts and monocytes. Calcif Tissue Int. 2003; 72:726–36.
15. Mayr H, Schlüfter S, Detsch R, Ziegler G. Influence of phase composition on degradation and resorption of biphasic calcium phosphate ceramics. Key Eng Mat. 2008;361–363:1043–6.
16. Daculsi G, Laboux O, Malard O, Weiss P. Current state of the art of biphasic calcium phosphate bioceramics. J Mater Sci Mater Med. 2003;14:195–200.
17. Hing KA. Bioceramic bone graft substitutes: influence of porosity and chemistry. Int J Appl Ceram Technol. 2005;2:184–9.
18. Karageorgiou V, Kaplan D. Porosity of 3D biomaterial scaffolds and osteogenesis. Biomaterials. 2005;26:5474–91.
19. Frosch K, Barvencik F, Viereck V, Lohmann CH, Dresing K, Breme J, Brunner E, Sturmer KM. Growth behavior, matrix production, and gene expression of human osteoblasts in defined cylindrical titanium channels. J Biomed Mater Res A. 2004; 68:325–34.
20. Liu D. Influence of porosity and pore size on the compressive strength of porous hydroxyapatite ceramic. Ceram Int. 1997; 23:135–9.
21. Rice RW. Comparison of stress concentration versus minimum solid area based mechanical property-porosity relations. J Mater Sci. 1993;28:2187–90.
22. Gibson LJ, Ashby MF. Cellular solids—structure and properties. 2nd ed. ed. Cambridge, UK: Cambridge University; 1997.
23. Zyman ZZ, Tkachenko MV, Polevodin DV. Preparation and characterization of biphasic calcium phosphate ceramics of desired composition. J Mater Sci Mater Med. 2008;19:2819–25.
24. Kwon S, Jun Y, Hong S, Lee I, Kim H, Won YY. Calcium phosphate bioceramics with various porosities and dissolution rates. J Am Ceram Soc. 2002;85:3129–31.
25. Guo G, Xu K, Han Y. The in situ synthesis of biphasic calcium phosphate scaffolds with controllable compositions, structures, and adjustable properties. J Biomed Mater Res B Appl Biomater. 2007;88A:43–52.
26. Raynaud S, Champion E, Lafon JP, Bernache-Assolant D. Calcium phosphate apatites with variable Ca/P atomic ratio III. Mechanical properties and degradation in solution of hot pressed ceramics. Biomaterials. 2002;23:1081–9.
27. Royer A, Viguie JC, Heughebaert M, Heughebaert JC. Stoichiometry of hydroxyapatite: influence on the flexural strength. J Mater Sci Mater Med. 1993;4:76–82.
28. Gauthier O, Bouler JM, Aguado E, Legeros RZ, Pilet P, Daculsi G. Elaboration conditions influence physicochemical properties and in vivo bioactivity of macroporous biphasic calcium phosphate ceramics. J Mater Sci Mater Med. 1999;10:199–204.
29. Wang X, Fan H, Xiao Y, Zhang X. Fabrication and characterisation of porous hydroxyapatite/β-tricalcium phosphate ceramics by microwave sintering. Mater Lett. 2006;60:455–8.
30. Puértolas JA, Vadilloa JL, Sánchez-Salcedoc S, Nietoc A, Gómez-Barrenae E, Vallet-Regí M. Compression behaviour of biphasic calcium phosphate and biphasic calcium phosphate–agarose scaffolds for bone regeneration. Acta Biomater. 2010. doi:10.1016/j.actbio.2010.07.032.
31. Deschamps AA, Claase MB, Sleijster WJ, de Bruijn JD. Design of segmented poly(ether ester) materials and structures for the tissue engineering of bone. J Control Release. 2002;78:175–86.
32. Deisinger U, Stenzel F, Ziegler G. Development of hydroxyapatite ceramics with tailored pore structure. Key Eng Mater. 2004;254–256:977–80.

33. Michna S, Wu W, Lewis J. Concentrated hydroxyapatite inks for direct-write assembly of 3-D periodic scaffolds. Biomaterials. 2005;26:5632–9.
34. Deisinger U, Irlinger F, Pelzer R, Ziegler G. 3D-Printing of HA-scaffolds for the application as bone substitute material. cfi-Ceram Forum Int. 2006;83:75–8.
35. Vorndran E, Klamer M, Klammert U, Grover LM, Patel S, Barralet JE, Gbureck U. 3D powder printing of b-tricalcium phosphate ceramics using different strategies. Adv Eng Mat. 2009;10:B67–71.
36. Deisinger U, Leiderer M, Detsch R, Hamisch S, Ziegler G. Extrusion freeform fabrication technique for tailoring hydroxyapatite scaffolds for bone tissue engineering applications. Cytotherapy. 2006;S2:15.
37. Simon JL, Michna S, Lewis JA, Rekow ED, Thompson VP, Smay JE, Yampolsky A, Parsons JR, Ricci JL. In vivo bone response to 3D periodic hydroxyapatite scaffolds assembled by direct ink writing. J Biomed Mater Res A. 2007;83:747–58.
38. Rumpler M, Woesz A, Varga F, Manjubala I, Klaushofer K, Fratzl P. Three-dimensional growth behavior of osteoblasts on biomimetic hydroxylapatite scaffolds. J Biomed Mater Res A. 2007;81:40–50.
39. Chu TM, Halloran JW, Hollister SJ. Hydroxyapatite implants with designed internal architecture. J Mater Sci Mater Med. 2001;12:471–8.
40. Deisinger U, Hamisch S, Schumacher M, Uhl F, Detsch R, Ziegler G. Fabrication of tailored hydroxyapatite scaffolds: comparison of a direct and an indirect rapid prototyping technique. Key Eng Mat. 2008;361–363:915–8.
41. Limpanuphap S, Derby B. Manufacture of biomaterials by a novel printing process. J Mater Sci Mater Med. 2002;13:1163–6.
42. Taboas JM, Maddox RD, Krebsbach PH, Hollister SJ. Indirect solid free form fabrication of local and global porous, biomimetic and composite 3D polymer-ceramic scaffolds. Biomaterials. 2003;24:181–94.
43. Chu TG, Warden SJ, Turner C. Segmental bone regeneration using a load-bearing biodegradable carrier of bone morphogenetic protein-2. Biomaterials. 2007;28:459–67.
44. Rumpler M, Woesz A, Dunlop JW, van Dongen JT, Fratzl P. The effect of geometry on three-dimensional tissue growth. J R Soc Interface. 2008;5:1173–80.
45. Deisinger U. Synthetisches Knochenersatzmaterial mit spongiosa-ähnlicher Struktur: Herstellung, materialwissenschaftliche Charakterisierung und biologisches Verhalten von Calciumphosphat-basierten Keramiken. Berlin: Mensch-und-Buch-Verlag; 2009.
46. Hattiangadi A, Bandyopadhyay A. Modeling of multiple pore ceramic materials fabricated via fused deposition process. Scripta Mater. 2000;42:581–8.
47. Tsukrov I, Kachanov M. Stress concentrations and microfracturing patterns in a brittle-elastic solid with interacting pores of diverse shapes. Int J Solids Struct. 1997;34:2887–904.
48. Carter DR, Haynes WC. The compressive behaviour of bone as a two-phase porous structure. J Bone Joint Surg Am. 1977; 59:954–62.
49. Detsch R, Uhl F, Deisinger U, Ziegler G. 3D-Cultivation of bone marrow stromal cells on hydroxyapatite scaffolds fabricated by dispense-plotting and negative mould technique. J Mater Sci Mater Med. 2008;19:1491–6.
50. Rumpler M, Woesz A, Dunlop JW, van Dongen JT, Fratzl P. The effect of geometry on three-dimensional tissue growth. J R Soc Interface. 2008;5:1173–80.